CHAPTER 1

Introduction to Chemically Derived Graphene

QIUJIAN LE[†a], TIAN WANG[†a], YUXIN ZHANG*[a] AND LILI ZHANG*[b]

[a]College of Materials Science and Engineering, Chongqing University, Chongqing 400044, China; [b]Institute of Chemical and Engineering Sciences, A*STAR, 1 Pesek Road, Jurong Island 627833, Singapore
*E-mail: zhangyuxin@cqu.edu.cn, zhang_lili@ices.a-star.edu.sg

1.1 General Background of Graphite and Its Derivatives

Graphite consists of a stack of graphene sheets, making it a three-dimensional carbon allotrope with two-dimensional lattice bonds. In each graphene layer, three of the four outer shell electrons in an individual carbon atom are bound to its three neighboring carbon atoms by strong sp^2 bonds (or sigma bonds), leaving one electron moving freely to define its conductivity. Relatively weak van der Waals interactions hold the graphene sheets together in the third direction, allowing the easy separation of layers of graphene sheets. Unlike the free electrons in metals, the free electrons, so-called π-electrons, in each graphene layer are able to move freely only on the atomic plane and thus graphene does not conduct in the direction perpendicular to the plane.

[†]These authors contributed equally to this book chapter.

Nanoscience & Nanotechnology Series No. 46
Chemically Derived Graphene: Functionalization, Properties and Applications
Edited by Jintao Zhang

Published by the Royal Society of Chemistry, www.rsc.org

After oxidization by Hummers,[1] Staudenmaier,[2] or Brodie's[3] methods, graphite layers are intercalated with water molecules, ions, and oxygen-containing functional groups, *i.e.*, hydroxyl, carboxyl, and carbonyl groups. As a result, the distance between layers is expanded and the van der Waals forces are weakened, facilitating further exfoliation processes. The oxidized product is known as graphite oxide. Monolayer graphite oxide, also known as graphene oxide, can be obtained by ultrasonication or vigorous stirring in the form of water-dispersible suspensions.[4] Chemically derived graphene (CDG) is finally obtained *via* reduction with various reducing agents, such as hydrazine,[5–8] sodium borohydride,[9,10] active metal,[11–13] reductive organics,[14–18] and some other methods.[19–23]

Graphite and its derivatives, such as graphite oxide, graphene oxide, and graphene, consist all of carbon atoms. However, they differ in terms of their atomic arrangement and chemical composition. Graphite is composed of a number of graphene layers, rendering it an excellent lubricant. Graphite oxide has a similar layered structure to that of graphite, but with a larger interlayer spacing (about two times that of the original graphite) owing to the intercalation of water molecules, functional groups, and ions. Due to the destruction of the conjugated structure in graphite by oxidation processes, graphite oxide exhibits poor electrical conductivity. However, the introduction of foreign molecules and oxygen-containing functional groups increases the hydrophilicity of graphite, facilitating subsequent processes in water-like environments. Graphene oxide refers to monolayer graphite oxide produced through the exfoliation of graphite oxide. It displays unique properties arising from the presence of rich functional groups, such as tunable solubility in a variety of solvents, controllable electrical and optical properties, and compatibility with organic and inorganic compounds to form composites. Graphene possesses much better electrical conductivity than graphene oxide. However, the obtained graphene still differs from the ideal material due to the defects and functional groups introduced during oxidation–reduction–exfoliation processes. Nevertheless, functionalized CDG holds great promise in electrocatalysis, photocatalysis, electrochemical energy storage and conversion, flexible devices, anti-corrosion, water purification, sensors, and many other areas. Perfect graphene refers to a defect-free two-dimensional single atomic layer of graphite. Numerous and excellent properties arise from its sp^2 hybridization and thin atomic thickness of 0.35 nm, such as a large theoretical specific surface area ($2630\ m^2\ g^{-1}$),[24] ultrahigh intrinsic charge carrier mobility of $200000\ cm^2\ V^{-1}\ s^{-1}$,[25] good optical transparency (~97.7%),[26] high Young's modulus (~1 TPa),[27] and excellent thermal conductivity ($3000–5000\ W\ m^{-1}\ K^{-1}$).[28] The properties of graphite and its derivatives are summarized and compared in Table 1.1.

This book will focus on the most recent and state-of-the-art progress on CDG materials and their applications. General fabrication methods and properties of CDG will be covered in the following sections. Challenges with respect to the technology, economics, and environmental concerns will be presented in the last section of this introductory chapter.

Table 1.1 Properties of graphite and its derivatives.

Product	Graphite	Graphene	Graphite oxide	Graphene oxide	Chemically derived graphene
Form	Layered structure (>10 layers)	Monolayer carbon atom	Layered structure with expanded interlayer spacing	Monolayer structure with many defects	Monolayer structure with some defects
	Powder form	Film	Paste/powder	Suspension/powder	Suspension/powder
Elemental composition	C	C	C, O, H	C, O, H	C, O, H
Density (g cm^{-3})	2–2.3	~0.77 mg m^{-2}	Depends on defects	Depends on defects	Depends on defects
Electrical conductivity (S m^{-1})	2–3 × 10^5 (in-plane) 3 × 10^2 (cross-plane)	10^6 (in plane)	Nearly insulator	Nearly insulator	4600–5880
Thermal conductivity (W m^{-1} K^{-1})	2000 (in-plane) 20 (cross-plane)	5300 (in-plane)	N/A	1.68–2.21 (in-plane)	61 (in-plane), 0.09 (cross-plane)
Young's modulus	N/A	1.06 TPa	N/A	290–470 GPa	6.3 GPa
Basic synthesis method	Exists in nature	Micromechanical exfoliation, chemical vapor deposition, epitaxial growth, chemically derived methods	Hummers method, Staudenmaier method, Brodie method	Thermal, chemical, electrochemical, exfoliation of graphite oxide	Chemical oxidation–exfoliation–reduction of graphite, liquid exfoliation, solid exfoliation by ball milling, intercalation–exfoliation
Main applications	Pencils, batteries, refractories, steel making, brake linings	Fundamental research, semiconductor, energy storage, screen, optoelectronic applications	Intermediate product of CDG, biomedicine, catalysis	Intermediate product of CDG, biomedicine, energy storage, catalysis, environmental protection, sensor, optoelectronic applications	Semiconductor, energy storage, catalysis, optoelectronic applications, biomedicine

1.2 Preparation Methods and State-of-the-art Research Progress

The main methods to produce CDG include the chemical oxidation–exfoliation–reduction of graphite, liquid exfoliation of graphite, solid exfoliation of graphite, intercalation–exfoliation of graphite, and bottom-up chemical assembly.[29] Figure 1.1 shows these typical methods for the mass production of CDG.[29] These methods differ in terms of the yield, efficiency, cost, properties of the product, and environmental impact. The achievement of uniform product quality with a green and sustainable process at low cost is a universal challenge.

1.2.1 Chemical Oxidation–Exfoliation–Reduction of Graphite

This method for the production of CDG involves the oxidation of bulk graphite, exfoliation of graphite oxide, and reduction of graphene oxide. There are three well-known oxidation methods: modified Hummers,[1] Staudenmaier,[2]

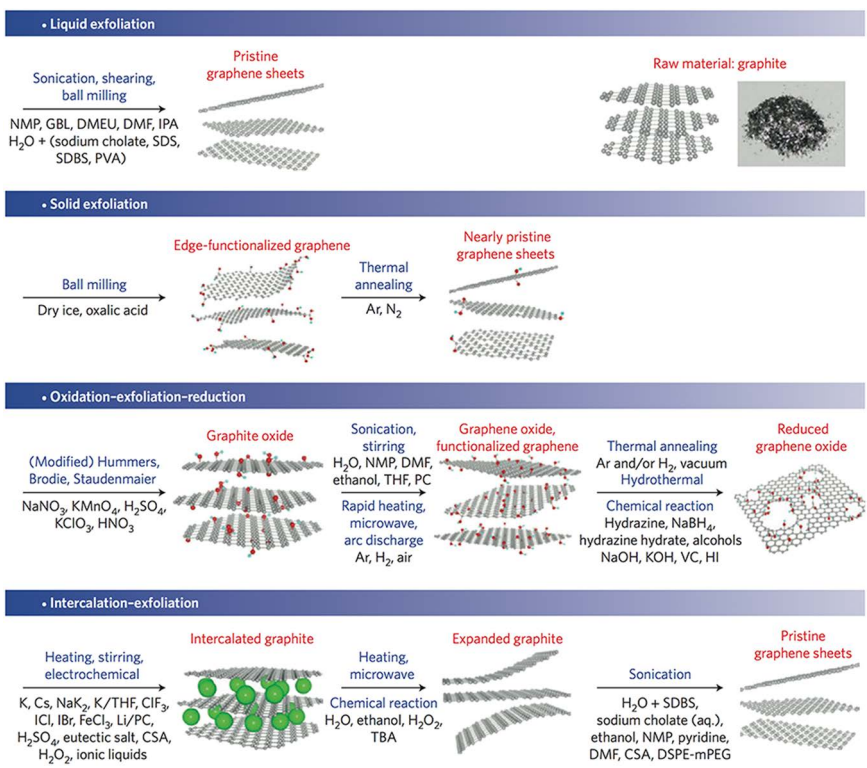

Figure 1.1 Four typical methods for the production of CDG. Reprinted by permission of Macmillan Publishers Ltd: *Nature Nanotechnology* (ref. 29), Copyright 2014.

and Brodie procedures.[3] All three methods involve the use of strong inorganic protonic acids (such as concentrated sulfuric acid, fuming nitric acid, or their mixtures) to intercalate small molecules within the graphite layers, followed by an oxidation reaction using $KMnO_4$, $KClO_4$, or other strong oxidants. Exfoliation of graphite oxide through ultrasonication or vigorous stirring results in graphene oxide and few-layer graphite oxide. CDG is finally obtained through a reduction process. Sometimes, exfoliation and reduction can be carried out in a single step.

Chemical, thermal, electrochemical, and hydrothermal reduction processes are the most commonly used reduction methods. In particular, chemical reduction is the most widely applied reduction method due to its simplicity, the possibility of large scale production, and good disparity in various solutions. A variety of organic and inorganic reducing agents have been used to reduce graphene oxide. Stankovich *et al.*[4,30] reported the successful reduction of graphene oxide with hydrazine monohydrate, providing a simple and feasible method for the mass production of CDG materials. However, significant agglomeration occurred upon reduction. To solve the agglomeration problem, Li *et al.*[31] reduced a graphene oxide aqueous solution using hydrazine hydrate under alkaline (pH = 10) conditions. The residual oxygen-containing functional groups of the reduced graphene oxide were ionized as negative charges under alkaline conditions. Thus, electrostatic repulsion prevents the π–π stacking of graphene sheets, resulting in uniformly dispersed aqueous solutions of CDG. In 2011, Zhou *et al.*[32] reported a rapid method to reduce graphene oxide with hydroxylamine at 90 °C, obtaining a dispersible CDG solution. Other reducing agents, such as hydroquinone,[14] sodium borohydride,[9] strong alkaline solution,[19] and hydroiodic acid,[21] have been explored as effective reagents to remove the oxygen-containing functional groups of graphene oxide.

In a typical thermal reduction process, graphite oxide or graphene oxide is heated rapidly under Ar or N_2 atmosphere, taking advantage of the pyrolysis of the oxygen-containing functional groups in the interlayer of graphite or on the surface of graphene oxide, releasing CO and CO_2 gases. Such gases force the graphite layers to expand rapidly overcoming the van der Waals forces between the layers, thereby achieving the exfoliation and reduction of graphite oxide in one step. The temperature of the thermal reduction has a great influence on the degree of reduction of graphite oxide. High temperatures of ~1000 °C afford a high degree of reduction. Electrochemical reduction removes the oxygen-containing functional groups from the surface of graphene oxide *via* an electrochemical process in a given buffer solution at room temperature. A high C/O ratio of 23.9 has been reported using this reduction method.[33] However, the complex preparation procedure for the working electrode and separation of the obtained CDG limit its wide application. Hydrothermal reduction takes place in an enclosed vessel, during which the pressure in the reactor increases with the temperature, and the solution can reach a temperature higher than the boiling point of the solvent. The oxygen-containing functional groups between the graphite oxide

sheets are removed, and chemically derived graphene is obtained. Zhou *et al.*[34] reported that supercritical water cannot only partially remove the oxygen-containing functional groups of graphene oxide but also recover part of the aromatic structure in the carbon lattice. A homogeneous graphene solution can be obtained under alkaline conditions (pH = 11), while agglomeration occurs under acidic conditions (pH = 3). Wang *et al.*[35] reported that the CDG obtained by hydrothermal reduction with DMF and hydrazine monohydrate as the solvent presented a higher C/O ratio than the one produced by chemical reduction with hydrazine monohydrate at atmospheric pressure.

1.2.2 Liquid Exfoliation

In a typical procedure of direct liquid exfoliation, graphite is firstly dispersed in a solvent or surface active agent, where enough surface energy can be gained to overcome the van der Waals forces between the graphene layers. Subsequently, the mixture is subjected to sonication or ball milling. Monolayer or few-layer graphene platelets are exfoliated from the graphite surface, leading to the production of CDG with good morphology and properties. Liquid exfoliation has advantages over other processes owning to its simple procedure and cheap production cost. Therefore, this method plays an important role in promoting the applications of graphene and its derivatives. According to the medium, liquid exfoliation can be divided into three categories: organic solvent-assisted exfoliation, surfactant-assisted exfoliation, and other exfoliation methods.

Successful exfoliation highly depends on the selection of the solvent. Liquid exfoliated graphene was obtained in organic solvent *N*-methylpyrrolidone (NMP) for the first time, and the as-prepared graphene presented little defects on the surface. Furthermore, almost all the graphene platelets obtained contained less than six layers. The drawback was that the concentration of the graphene suspension was relatively low, only 0.01 mg mL^{-1}. Ionic liquids have a surface energy close to that of graphene, which is a key prerequisite for the direct exfoliation of graphite in a solvent. The first successful application of ionic liquids in the liquid exfoliation of graphite was achieved with 1-butyl-3-methyl imidazolium[36] salts. The concentration of the as-prepared graphene suspension was 0.95 mg mL^{-1} (ultrasonication for 1 h), and most graphene platelets were less than five atomic-layer thick. It is worth noting that the concentration of graphene achieved in 1-methyl-3-butylimidazolium hexafluorophosphate was up to 5.3 mg mL^{-1} with an average thickness of the graphene platelets of 6–7 atomic layers.[37] Despite the low content of monolayer graphene, ionic liquids do produce stable high-concentration CDG suspensions.

The solvents discussed above are not volatile, which cause problems for subsequent processes. This makes it difficult to remove the solvent when fabricating graphene as thin films or composite materials.[38] In general, the presence of residual solvents can significantly affect the performance of the power measurement equipment and thus, complete removal of the solvent is

highly required. Therefore, the preparation of CDG in low boiling-point solvents is more promising. So far, liquid-phase exfoliation in low boiling-point solvents has been rarely reported. Coleman *et al.*[39] described the separation of graphene in low boiling-point solvents such as chloroform, acetone, and isopropanol. Under optimum conditions, the highest concentration of a graphene suspension reached 0.5 mg mL^{-1}. Despite the rapid development of liquid-phase exfoliation in recent years, many obvious problems still exist. Among them, the most important one is the relatively low concentration of the obtained CDG dispersions. Better exfoliation efficiency can be obtained by adding inorganic salts, organic salts,[40,41] or other auxiliary agents, or by increasing the ultrasonication time. For example, the exfoliation efficiency was significantly improved upon addition of inorganic NaOH in NMP, *N*,*N*-dimethylacetamide, and cyclohexanone. The concentration of a graphene suspension in cyclohexanone was 20 times larger after addition of NaOH.[40]

1.2.3 Solid Exfoliation by Ball Milling

Ball milling is a common technology in the powder production industry. For most ball mill equipment, two methods can be used for peeling and grinding. The first one is shear stress, which is considered to be a good mechanical path for exfoliation. This method allows the fabrication of graphene sheets with large size. The second one is the vertical impact of the ball during rolling, which can shatter graphene sheets and sometimes shatter crystalline structures into amorphous or unbalanced phases. Therefore, it is desirable to reduce such vertical impact during the fabrication process in order to obtain high-quality large-size graphene.

At first, ball milling was only used to reduce the size of graphite. This method was not further explored until the first report on the liquid-phase exfoliation of graphite in 2010. Knieke *et al.*[42] and Zhao *et al.*[43] improved the ball milling procedure, making it capable of producing graphene materials. Similar to liquid exfoliation, chemically inert inorganic salts are mixed with graphite to weaken the van der Waals forces so as to achieve the exfoliation of monolayer or few-layer graphene platelets from graphite. Leon *et al.*[44] reported a method to exfoliate graphite based on the interaction of graphite with solid melamine. Jeon *et al.*[45] described an approach to functionalize the edges of graphene at large scale *via* solid exfoliation of graphite. Graphite was mixed with hydrogen, carbon dioxide, sulfur trioxide, or a gas mixture containing carbon dioxide and sulfur anhydride, followed by a dry milling process. Under different humidity conditions, a variety of functionalized graphene sheets were obtained. According to another study by Jeon,[46] after grinding the original graphene sheets with dry ice for 48 h, smaller graphite particles (100–500 nm) functionalized with sulfonic groups were successfully obtained, which could be highly dispersed in various solvents and further exfoliated into single-layer or several-layer graphene nanosheets (GNSs) with high quality. Although the ball-milling method is regarded as an effective method for the large-scale preparation of graphene, the decomposition of

the ball milling medium still cannot be ignored. On the other hand, ball mill-assisted solid exfoliation requires high energy input and the structure integrity of the resultant CDG may be damaged. Studies have shown that decomposition cannot be completely avoided during the milling process. Thus, fragmentation and defects are unavoidable. However, this could be a double-edged sword in the preparation of CDG. On the one hand, it can be used to functionalize graphene and improve the exfoliation efficiency; on the other hand, the size of CDG can be tailored by such ball milling processes.

1.2.4 Intercalation–Exfoliation

Direct liquid exfoliation has the drawbacks of low efficiency and the tendency of restacking of graphene layers during the subsequent solvent removal process. Meanwhile, in ball milling-assisted solid exfoliation, a large amount of energy input is required, which may damage the structural integrity of the obtained CDG. As a result, the method of intercalation–exfoliation was developed to first intercalate and expand the graphite layers through non-covalent bonding. This facilitates the subsequent exfoliation step and produces CDG with fewer functional groups and defects. Compared to the direct liquid-exfoliation method, intercalation–exfoliation is carried out in a solid phase system that avoids the dispersion of graphite and thus simplifies the process. Moreover, unlike ball milling-assisted solid exfoliation, the interlayer spacing is greatly expanded thanks to the intercalation process, facilitating the exfoliation.

Non-oxidative intercalation–exfoliation of graphite by Bronsted acids has been reported.[47] The intercalation is achieved by acid–base chemistry rather than electron transfer reactions and dipolar interactions exist between the guest molecules and the polarizable graphene sheets. It is important that the guest molecule activity exceeds a threshold value for the intercalation to occur. Subsequently, the intercalated graphite is readily exfoliated in dimethylformamide to give a suspension of crystalline single- and few-layer graphene sheets. Low-temperature exfoliation of graphite was achieved with $FeCl_3$ and nitromethane (CH_3NO_2) co-intercalated graphite under microwave heating.[48] In this case, $FeCl_3$ served as a mild oxidant to facilitate the intercalation of CH_3NO_2 into graphite while maintaining the integrity of the graphene layers. Under microwave heating, CH_3NO_2 decomposes, and gases such as NH_3, HCOOH, NO_2, H_2O, and CO_2 are generated, which further expand and exfoliate graphite into CDG with a low degree of defects and functional groups. Okotrub *et al.*[49] treated fluorinated graphite intercalated with acetonitrile (CH_3CN) or isopropylamine ($(CH_3)_2CHNH_2$) at 800 °C to prepare edge-functionalized graphene materials. During the heat treatment, acetonitrile or isopropylamine decompose into HF, C_2F_4, and CF_4, which expand the graphite structure into graphene. Meanwhile, nitrogen species are left on the edge of the obtained graphene in the form of pyridinic and protonated nitrogen.

In addition to the annealing method, electrolytic exfoliation has also been investigated to prepare CDG. Huang *et al.*[50] reported the preparation of CDG

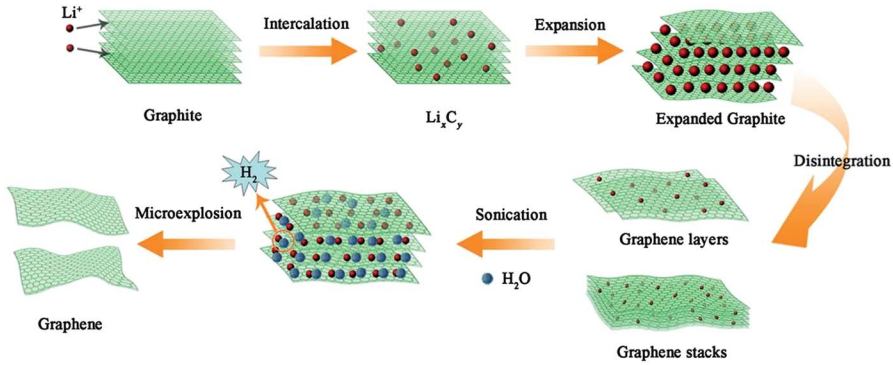

Figure 1.2 Synthesis of graphene sheets through the Li intercalation–expansion–microexplosion process. Reproduced from ref. 50 with permission from the Royal Society of Chemistry.

via molten salt electrolytic exfoliation based on a Li-ion intercalation–expansion–microexplosion mechanism. It should be noted that this electrolytic exfoliation process is different from the liquid exfoliation method. Exfoliation in a liquid is based on interlayer oxidation and ion intercalation, which may lead to the oxidation of graphite and the introduction of defects and structural damage. However, electrolytic exfoliation of graphite occurs in the form of a graphite cathode avoiding such oxidation problems completely. The mechanism is based on Li-ion intercalation–expansion–microexplosion, as depicted in Figure 1.2. The intercalation of Li ions occurs in the same electrolysis cell, avoiding the additional synthesis of graphite intercalation compounds.[48,49] Besides, intercalation compounds (Li_xC_y) are produced through the direct *in-situ* reduction of graphite, eliminating the possibility of oxygen-containing functional groups. With the abundant introduction of Li ions, the disintegration of graphite occurs to form graphene layers and stacks. Finally, the solid electrolyte is placed in water under ultrasonic treatment, and sufficient hydrogen is released to further exfoliate the graphene layers.

1.2.5 Large-scale Manufacturing Processes

A very recent review by Professor Zhu *et al.*[51] has given a comprehensive and most updated summary of the industrial-scale production of graphene materials and its related issues. Among the many methods introduced above, the large scale industrial production of CDG is mainly based on liquid exfoliation, chemical oxidation–exfoliation–reduction, and intercalation–exfoliation of graphite. Liquid exfoliation has the advantage of its simple procedure; however, the CDG obtained thereafter often presents multi-layers and suffers from residue contamination from the process. Though defects and agglomeration are the major drawbacks of the chemical oxidation–exfoliation–reduction method, it is still considered one of the most effective methods for the

large production of CDG at low cost. In addition, the intermediate product, graphene oxide, contains rich functional groups. It can be used as a reagent or be further modified with organic or inorganic materials, thus expanding the applications of CDG materials.

Prof. Cheng Huiming from the Institute of Metal Research, Chinese Academy of Sciences, has implemented the manufacture of graphene in large scale *via* chemical vapor deposition (CVD) and graphite intercalation methods. Moreover, chemical oxidation–reduction and graphite intercalation methods are being used to prepare graphene on a large scale at Beijing Shengmeng Technology and Changzhou Sixth Element Co. Ltd. At present, most companies are able to synthesize graphene flakes on a several-kilogram scale. Some large companies are able to make several tons of graphene flakes annually, such as Changzhou Sixth Element, Beijing Shengmeng Technology, Beijing Carbon Century Co. Ltd., *etc*.

1.3 Properties of Chemically Derived Graphene

1.3.1 Physical Properties

Compared to graphene prepared *via* mechanical exfoliation or CVD, CDG presents some defects and residual functional groups, leading to an imperfect planar structure. However, flexible synthetic processes are able to produce CDG with different morphologies, tunable sizes, large surface area, and controllable porous structures. Particularly, porous CDG presents advantages in a wide range of applications, including electronic devices, energy storage, and sensors. Porous CDG possesses a large surface area, pore volume, and good wettability in the electrolyte, besides other inherent properties of CDG. One common approach to fabricate porous CDG is through chemical and physical activation.[52] A fraction of the carbon acts as a sacrificial reductant to release gases, leaving behind micro and mesopores. However, the relatively low yields and packing densities are the major concerns for porous CDG. CDG powders and papers with a large surface area close to the theoretical value have been achieved by chemical activation.[53,54] A HNO_3-assisted mechanical cavitation–chemical oxidation method was used to prepare holey graphene paper, delivering remarkable enhanced rate capability in Li-ion batteries.[55] Highly densified CDG is required in applications such as energy storage and conversion.[56] Strategies to obtain CDG with high density include the appropriate assembly of graphene sheets and incorporation of other active materials. Porous CDG films with a density of 1.33 g cm^{-3} were obtained through vacuum filtration.[57] Another work by Yang reported the fabrication of CDG with a density of about 70% that of raw graphite by an evaporation-induced drying process. Although substantial efforts have been devoted to the fabrication of CDG with various morphologies and structures, precise control over parameters such as the size of the CGD sheets, pore size, and pore-size distribution is still challenging, especially for large-scale production and batch production.

1.3.2 Chemical Properties

The defects and rich functional groups on the surface and edges of CDG determine its chemical reactivity toward many organic and inorganic molecules in a variety of reaction systems. Therefore, the functionalization of CDG with different types of materials, such as polymers, metals, metal oxides, ceramics, and many others, has been widely studied. The functionalization of CDG for applications in electrochemistry, energy storage and conversion, catalysis, anti-corrosion, separation, and purification is the main focus of this book. Some composites based on CDG have already been commercialized. For example, CDG-based zinc anti-corrosion primers are produced in up to 5000 tons per annum since 2017.[51]

1.3.2.1 Functionalization with Polymers

An early work describes a clever way to functionalize CDG with conducting polymer (polyaniline) nanofibers, *via* an *in-situ* polymerization method, followed by designed reduction and reoxidation steps. The homogeneous CDG–polymer composites exhibit good energy storage performance.[58,59] The preparation of CDG–polymer composites usually focuses on the uniform dispersion of CDG in matrix composites, which maximizes the interfacial contact between CDG and the polymer matrix, prevents CDG agglomeration, and leads to improved performances. Similar to conventional polymer preparation methods, the main synthesis methods of CDG–polymer composites include *in-situ* polymerization, solution mixing, and melt blending.[60]

1.3.2.2 Functionalization with Ceramic Matrices

Conventionally, one-dimensional carbon fiber, carbon nanotubes, and ceramic whiskers are used in ceramic matrices to form ceramic reinforcements. However, aggregation greatly restricts the application of these composite materials. Compared to low-dimensional nanocomposites, CDG offers advantages such as good dispersion in ceramic matrices, and excellent mechanical and physical properties. Although CDG holds great potential to enhance some specific properties of CDG–ceramic composites, only a few studies exist on the preparation of CDG-based ceramic reinforcements. CDG–alumina[61] and graphite–silicon nitride[62] composites were fabricated by a powder processing method. In this method, CDG was firstly dispersed with the assistance of ultrasonic treatment. Then, the dispersed CDG was mixed with ceramic powder. Ball milling or a high-energy ball-milling method was used to obtain a well dispersed CDG–ceramic mixture. Wang[63] produced well dispersed CDG–ceramic composites using heterogeneous coagulation with CDG colloidal solutions in water.

Research has shown that CDG cannot only significantly improve the electrical properties of ceramic composites, it can also enhance its mechanical properties, especially in regard to fracture toughness. The introduction of

CDG in a ceramic matrix can refine the grain size, form a dense structure, and hinder the crack propagation. Ceramic composites with good electrical conductivity have great significance in functional ceramics. Ramirez[64] prepared Si_3N_4–CDG block composites through spark plasma sintering (SPS). Si_3N_4 composites containing 25% graphene nanoplatelets (GNPs) delivered a high conductivity of 40 S cm^{-1},[65] much higher than that of other conductive ceramic particles or ceramic composites.

1.3.2.3 Functionalization with Metals

Two approaches exist to prepare CDG–metal composites: (1) functionalization of CDG with metal nanoparticles to improve its activity and dispersibility; this kind of functionalized CDG has applications in fields such as catalysis,[66–73] sensing,[74,75] and spectroscopy;[76–78] and (2) functionalization of a metal matrix with CDG to improve the mechanical properties of the metal while maintaining its thermal and electrical properties.[78–80]

Dispersing metal nanoparticles on CDG can prevent agglomeration of the metal nanoparticles, enhancing the overall efficiency and activity. Meanwhile, this strategy can significantly reduce the amount of precious metals required and improve the stability of the composites. Methods including wet chemistry,[73,76] electrochemistry,[70,75] self-assembly,[74,81] hydrothermal, and microwave-assisted[67,82] syntheses have been developed for the preparation of CDG–metal composites. CDG functionalized with gold nanoparticles was firstly reported by Muszynski.[83] This work introduced a basic method to functionalize CDG with noble metal nanomaterials, stimulating a surge of studies in this field. CDG functionalized with single metal and bimetallic nanoparticles is a hot topic, especially in the field of catalysis. The main challenge in the functionalization of CDG with bimetallic nanoparticles lies in the structure and component control of the bimetallic nanoparticles on the surface of CDG. The success in the large scale production of CDG–single metal and bimetallic nanoparticles will have a great impact on the field of catalysis. The significant reduction of precious metal loadings and ultralow metal contents (ppm) will impact the efficiency and sustainability of catalytic processes and advance the manufacturing and engineering sectors, especially for the food, personal care, and pharmaceutical industries.

As for metal matrices reinforced with graphene, Jeon *et al.*[79] developed graphene–aluminum metal matrix composites *via* friction stir processing. A GO suspension and Al alloy sheets served as raw materials, followed by the experimental steps shown in Figure 1.3. Thermal gravimetric analysis (TGA) results showed that the oxygen-containing functional groups, for example hydroxyl, carbonyl, and carboxyl, had been converted into CO, CO_2, and H_2O, obtaining reduced graphene oxide with high thermal conductivity. The following thermal conductivity analysis indicated that these graphene–aluminum metal matrix composites delivered a high thermal conductivity of 171.7 W m^{-1} K^{-1} at a temperature of 250 °C, which is 15% higher than that of the original Al alloy. Moreover, the ductility of the prepared metal matrix composites can also be improved thanks to the reinforcement with graphene.

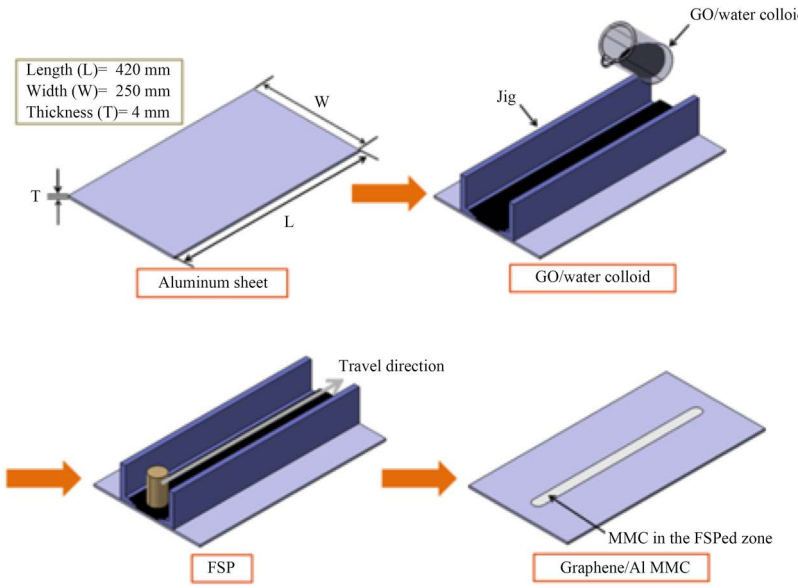

Figure 1.3 Schematic diagram of metal matrix composite fabrication by friction stir processing. Reproduced from *International Journal of Precision Engineering and Manufacturing*, Material properties of graphene/aluminum metal matrix composites fabricated by friction stir processing, **15**, 2014, 1235–1239,[79] C.-H. Jeon, Y.-H. Jeong, J.-J. Seo, H. N. Tien, S.-T. Hong, Y.-J. Yum, S.-H. Hur and K.-J. Lee, © KSPE and Springer 2014, with permission of Springer.

1.3.2.4 Functionalization with Metal Oxides

A variety of CDG–metal oxide composites have been prepared and investigated, such as V_2O_5,[84,85] Fe_3O_4,[86–88] MnO_2,[89–91] Co_3O_4,[92–94] SnO_2,[95,96] *etc*. The obtained nanocomposites combine the advantages of the large specific surface area of CDG and high electrochemical activity of the metal oxides, making them good candidates for applications in energy storage and sensing. The fabrication of CDG–metal oxide composites can be divided into *ex-situ* and *in-situ* approaches.

In *ex-situ* methods, metal oxide nanoparticles and graphene are separately synthesized. CDG–metal oxide composites are formed after mechanical mixing of the two materials, whereby the metal oxide nanoparticles and graphene are linked to each other through either covalent or non-covalent bonding (π–π interactions, van der Waals forces, hydrogen bonding, and electrostatic interactions). However, both metal-oxide nanoparticles and graphene need to be functionalized in order to initiate the formation of chemical bonds, which makes this method a little complex. On the other hand, the metal oxide and graphene are synthesized separately without interference. Thus, it is relatively easy to control certain properties such as the size, morphology, and density of the metal-oxide nanoparticles.[97,98] The ionization of oxygen-containing functional groups endows GO and CDG with negative

charges, which readily interact with metal oxide nanoparticles carrying positive charges. Based on this mechanism, Fe_3O_4–rGO[99] and MnO_2–rGO[100] nanocomposites were synthesized by mixing graphene (negatively charged) and the metal oxide (positively charged).

Although *ex-situ* methods can lead to the fabrication of CDG–metal oxide composites with different features, the low density and uneven distribution of metal-oxide nanoparticles on CDG[101] greatly hinder the properties of the nanocomposites. *In-situ* methods enable the functionalization of GO or CDG with typical nucleation sites, leading to the uniform distribution of metal oxide nanoparticles on graphene. *In-situ* methods that have been developed include (but are not limited to) hydrothermal, electrochemical deposition, and other methods. Among them, the hydrothermal method is the most popular approach for the synthesis of CDG–metal oxide composites. The high temperature and pressure applied greatly enhance the reaction activity and eliminate the subsequent annealing process. Thus, the crystallinity of the obtained metal oxide nanoparticles can be improved in one step, enhancing their electrochemical properties. In fact, almost all CDG–metal oxide composites can be prepared through such a hydrothermal method. Ye[88] reported a simple hydrothermal method to synthesize Fe_3O_4-functionalized graphene materials. Firstly, graphene oxide, $FeCl_3{\cdot}6H_2O$, and $FeCl_2{\cdot}4H_2O$ were dissolved in water in the presence of ammonia. After the hydrothermal reaction, Fe_3O_4-functionalized CDG with uniform size (35–45 nm) was obtained. Wang *et al.*[102] developed a two-step hydrothermal method to functionalize rGO with $Ni(OH)_2$, whose morphology could be easily controlled by varying the reaction temperature and degree of oxidation of rGO. Moreover, the electrochemical deposition method has also attracted much attention due to its low cost, high stability, and environmentally friendliness. In a typical procedure, graphene or CDG is firstly coated on an electrode and placed in an electrolyte containing a metal precursor solution. Upon application of a certain potential, the metal oxide is deposited on the surface of graphene or CDG. Using the electrochemical deposition method, MnO_2–rGO,[103] Fe_3O_4–CNT–rGO,[104] and Co_3O_4–rGO[105] nanocomposites were prepared in different electrolytes. In addition, the sol–gel method is another popular approach to fabricate CDG–metal oxide composites. For instance, TiO_2–rGO was synthesized by a sol–gel method, delivering remarkable electrochemical properties for sodium-ion batteries and high photocatalytic efficiency for pollutant photodegradation.[106]

1.3.3 Thermal Properties

The thermal properties of graphene play an important role in electronics due to its intrinsic high anisotropic thermal conductivity, where the high in-plane thermal conductivity (K) is able to conduct heat away from a hot spot in the in-plane direction, while low cross-thermal conductivity (Kc) protects the underneath layers from heating. Due to the strong covalent bonding between carbon atoms, the phonon conducting model plays a major role in

the thermal conductivity of graphene. Phonon conduction is highly affected by the mean free-path of phonons, determined by phonon–phonon scattering and defect scattering resulting from the interactions between phonons and edges, grain boundaries, and heteroatoms. High quality bulk graphite displays an in-plane thermal conductivity of 2000 W m^{-1} K^{-1} and cross-plane thermal conductivity of 20 W m^{-1} K^{-1} at room temperature.[107,108] However, its non-flexible nature restricts its industrial application. The relationship between the thermal conductivity of graphene and the temperature was studied by Berber,[109] who found that the thermal conductivity of monolayer graphene decreased with the increasing temperature between 200–400 K. Moreover, with the increasing number of graphene layers, the enhancement of phonon scattering and interactions between graphene layers led to the reduction of the graphene thermal conductivity by an order of magnitude to the graphite level. In Nika's work,[110] the thermal conductivity of monolayer graphene was highly determined by the size, defect concentration, and edge roughness of graphene, and an approximate range of 2000–5000 W m^{-1} K^{-1} was reported. Hao *et al.*[111] further investigated the impact of monatomic defects and Stone–Wales dislocation on the thermal properties of graphene *via* molecular dynamics simulation. An 'obvious' conclusion was drawn that the thermal conductivity decreased rapidly with the increasing defect concentration, which could be explained by phonon scattering. In addition to the theoretical calculation and numerical simulation, experimental work was carried out to determine the thermal properties of suspended graphene and supported graphene materials. Due to substrate effects, the obtained thermal conductivities of suspended and supported graphene were different. The first experimental determination of the thermal conductivity of suspended single-layer graphene was reported by Balandin in 2008.[28] Mechanical exfoliated graphene was suspended on a Si/SiO_2 substrate, followed by irradiation with a confocal micro-Raman laser. Based on the function correlation between the temperature coefficient and thermal conductivity, a thermal conductivity in the range from $(4.84 \pm 0.44) \times 10^3$ to $(5.30 \pm 0.48) \times 10^3$ W m^{-1} K^{-1} was estimated. Even graphene supported on SiO_2 showed a high thermal conductivity of 600 W m^{-1} K^{-1}, exceeding that of some metals such as copper and conventional thin-film electronics.[112] Most of the thermal properties measured or predicted are based on graphene produced by mechanical exfoliation or CVD to ensure high quality and perfect structure. In view of the large defect densities and foreign elements on CDG, the corresponding thermal properties are expected to be inferior to those of mechanically exfoliated and CVD graphene. Nevertheless, the relatively low cost and efficient large-scale production of CDG makes practical its applications as filler in thermal interfacial materials. CDG materials are more promising than carbon nanotubes as fillers owning to their superior thermal coupling to the matrix and lower cost. Up to a 400 times increase in the thermal conductivity of PET was reported when a graphene laminate, a densely packed CDG material, was used as the filler.[113] Annealing of free-standing CDG films at high temperature (1000 °C) afforded films with exceptionally strong anisotropic

thermal conductivity, $K/Kc \approx 675$, which is substantially larger than that of high-quality graphite.[114] These experimental results point to the promising thermal properties of CDG for application in thermal management.

1.3.4 Electrical Properties

There is a classical saying in materials science that the properties of a certain material highly depend on its structure. It is natural to discuss the structure of graphite and its derivatives when discussing their properties. Although graphite has long been known as a good conductor, its electrical properties are far inferior to those of graphene. Graphite is composed of many layers of graphene, where each atom in the layer connects to another three atoms by covalent bonding. The π–π conjugated structure formed by the fourth electron ensures the high conductivity of graphite. On the other hand, the unique carrier type and massless Dirac fermions in graphene are two of its most significant properties, leading to its excellent electrical properties. Generally speaking, graphite with a number of layers below 10 can be denoted as a CDG material. Thus, the number of graphene layers has a great impact on the properties, especially the electrical properties, of the obtained CDG. In addition, the degree of reduction, amount, and location of residual functional groups greatly influences the electrical properties of CDG.

In addition to the impact of the number of graphene layers, the residual functional groups and defects also influence the electrical properties of CDG to a great extent. The specific oxidation and reduction processes will determine the amount and location of residual functional groups, leading to different carbon to oxygen ratios. Punckt and co-workers[115] studied the effects of the functional groups on the electrical properties of CDG obtained *via* thermal exfoliation and reduction at different temperatures. CDG materials with different degrees of reduction were obtained. The resistance decreased from 400 kΩ sq^{-1} to less than 10 kΩ sq^{-1} at increasing C/O ratios from 7.3 to 340. Apart from the changes in the resistance, the type of current–voltage curves also changed from non-Ohmic to typical Ohmic behavior. During the reduction of graphene oxide to CDG, the π–π conjugated structure was gradually restored. Meanwhile, the electron transport also changed from hopping to diffusive motion, which is primarily restricted by the scattering of functional groups and defects. Punckt's work revealed the relationship between the C/O ratio and the electrical properties of graphene without considering the type of functional groups. The influence of the type of functional groups (epoxide or hydroxyl) on the electrical properties of graphene were studied by Yan *et al.*[116] First-principles calculation showed that individual functional groups (epoxide or hydroxyl) lead to a special electronic bound state, which has a great influence on the transportation properties of CDG. When epoxide and hydroxyl groups co-exist, these two functional groups tend to aggregate with each other on the CDG plane. Chain-like structures may form *via* hydroxyl groups in close proximity to epoxide moieties *via* hydrogen bonding. Moreover, the degree of reduction together with the content of epoxide or hydroxyl

groups have a significant impact on the energy gap of CDG, which is also an important parameter for the electrical properties.

1.3.5 Electrochemical Properties

The expanded interlayer distance, rich functional groups, and improved hydrophilicity provide CDG with good contact with the electrolyte and excellent electrochemical properties.

Two kinds of charge storage mechanisms exist in supercapacitors: the electrical double layer (EDL) and pseudo-capacitive mechanisms. The EDL capacitance arises from the adsorption and desorption of charges on the interface of the electrolyte and electrode, which highly relies on the specific surface area and porous structure. Pseudo-capacitance originates from fast and reversible Faradaic reactions taking place at the electrolyte–electrode interface or at the region of the electrode near the surface. The pseudo-capacitance relies on the electroactive species on the electrode materials. Porous CDG materials are suitable as electrode materials for EDL capacitance because of their high surface area and good conductivity. The electrochemical properties of CDG were firstly reported by Ruoff's group.[117] Specific capacitances of 135 and 99 F g^{-1} were obtained in aqueous and organic electrolytes, respectively. In addition to the functional groups giving rise to additional pseudo-capacitance, CDG with dopants such as nitrogen presents enhanced capacitance. Zhang *et al.*[118] showed that the area-normalized capacitance of lightly nitrogen-doped activated graphene with similar porous structures increased from 6 μF cm^{-2} to 22 μF cm^{-2} for 0 at% and 2.3 at% N-doping, respectively. The increase in bulk capacitance with the increasing nitrogen concentration and the increase of interfacial capacitance in the N-doped monolayer graphene *versus* pristine monolayer graphene suggested that the increase in the EDL-type capacitance of many, if not all N-doped carbon electrodes, is primarily due to the modification of the electronic structure of graphene by the N-dopant. It was further found that the quantum capacitance is closely related to the N-dopant concentration and that N-doping provides an effective way to increase the density of states of monolayer graphene.[119] Graphite, with a theoretical capacity of 370 mA h g^{-1}, is a practical anode material for Li-ion batteries (LIBs) because of its good cyclic stability. CDG displays a similar intercalation mechanism to that of graphite according to Pollak's research, but with a much higher reversible capacity.[120] Thus, CDG materials have been widely studied to replace conventional graphite materials in recent years. Similar to the intercalation mechanism in graphite, the inter-layer distance has a significant impact on the lithium storage properties of CDG. Yoo and co-workers[121] found that GNSs delivered a good specific capacity of 540 mA h g^{-1}, while the capacity increased to 730 and 784 mA h g^{-1} upon introduction of CNTs and C60 macromolecules in the interlayer space of the GNSs, respectively. A higher capacity of 1054 mA h g^{-1} was reported on disordered GNSs.[122] The highly disordered structure and defects were believed to reduce the electrical conductivity of graphene,

making it a poorer material for electronic devices. However, the potential of disordered graphene in LIBs was explored due to its high reversible capacity (over 1000 mA h g^{-1}) and stable cycling performance. The capacity enhancement of disordered graphene was attributed to the additional active sites for reversible storage provided by defects and edges with high electrochemical activity. On top of the defects and edges, other factors such as the surface area, porous structure, and functional groups also highly affect the lithium storage properties of CDG.

CDG also shows promising applications as the electrode for the oxygen reduction reaction (ORR). Currently, Pt/C remains the electrode of choice for the ORR owing to its high electrochemical activity and efficiency. However, the high cost, low abundance, poor durability, and CO deactivation of the catalyst have greatly hindered the development of fuel cells for commercial applications. N-doped graphene has delivered high ORR activity *via* a four-electron transfer process.[123] Zhang *et al.* have shown that the ORR is a four-electron transfer process in N-doped graphene.[124] Their work also pointed out that pure graphene has no electrocatalytic activity for the ORR and that doping of graphene with foreign elements is necessary. The ORR can occur spontaneously in N-doped graphene. Upon introduction of hydrogen into the ORR system, a series of reactions take place step-by-step, including the formation of C–O bonds between graphene and oxygen, cleavage of the O–O bonds, and generation of H_2O molecules. According to simulation results, the electrocatalytic active sites on N-doped graphene rely greatly on the spin density distribution and atomic charge distribution. As a matter of fact, non-paired electrons are introduced into N-doped graphene, changing the atomic charge distribution due to the introduction of nitrogen atoms on the graphene lattice. Researchers believe that carbon atoms with the highest spin density are the sites with the highest electrocatalytic activity. Moreover, if the value of the spin density is negative enough, carbon atoms bearing a large positive atomic charge density may also act as electrocatalytic active sites. In addition to nitrogen doping, other elements have also been studied for graphene doping for enhanced electrocatalytic activity, such as boron,[125] phosphorus,[126] iodine,[127] and sulfur.[128,129] The enhancement of the electrocatalytic activity in the ORR is restricted by the relative low content of doping elements. Dual-element doping has been widely studied to improve the catalytic activity for the ORR,[130–132] allowing not only for an increase of the content of doping atoms, but also strengthen the synergetic effects between dopants. Sulfur and nitrogen dual-doped graphene showed superior catalytic properties than sulfur- or nitrogen-doped graphene.[130] Owing to the good coordination between nitrogen and sulfur, both dopants were fully utilized for the ORR, avoiding the formation of inactive components in dual-doped graphene. In short, although pure graphene does not have any catalytic activity for the ORR, heteroatom-doped graphene delivers good activity and is thus a promising electrode material for fuel cells.

1.3.6 Mechanical Properties

The Young modulus of monolayer graphene has been calculated to be 1.05 TPa by molecular dynamics simulation,[133] which is close to the value obtained from first principles calculations (1.11 TPa).[134] Huang *et al.*[135] pointed out that the tensile and bending stiffness can be directly calculated from the interatomic potential, which is related to the load type, making the Young modulus non-constant. Experiments have been carried out to measure the Young modulus. However, the small size of CDG results in large uncertainties in the experimental measured values. At present, experimental methods to determine the Young modulus include tip-induced deformation,[136,137] bulge test,[138,139] and atomic force microscopy (AFM)-assisted nanoindentation[27,140] methods. Figure 1.4 shows a schematic diagram of these three methods. In the tip-induced deformation method, graphene is firstly fixed on a substrate with the middle part suspended, followed by applying a load on the middle section of the graphene beam. The spring constant is obtained to further calculate the elastic modulus. The Young modulus of mechanical exfoliated graphene and CDG obtained by this method were 0.5 TPa[137] and 0.25 TPa,[136] respectively. The results indicate a negative impact of the defects and functional groups on the mechanical properties of graphene. However, the inner tension in CDG is significantly lower than that of mechanical exfoliated graphene, indicating its high flexibility. Bulge tests were firstly reported by Vlassax and Nix[138] to determine the mechanical properties of films. Specifically, the film is adhered on a micro pit to form

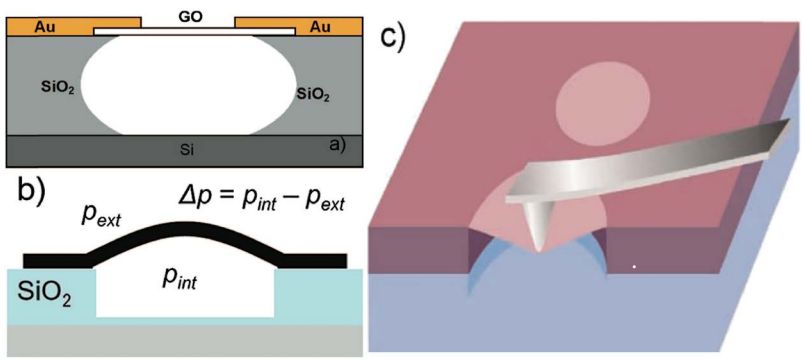

Figure 1.4 Schematic diagrams of (a) tip-induced deformation, (b) bulge test, and (c) AFM-assisted nanoindentation. (a) Reprinted with permission from C. Gómez-Navarro, M. Burghard and K. Kern, *Nano Letters*, 2008, **8**, 2045–2049.[136] Copyright 2008 American Chemical Society. (b) Reprinted with permission from J. S. Bunch, S. S. Verbridge, J. S. Alden, A. M. v. d. Zande, J. M. Parpia, H. G. Craighead and P. L. McEuen, *Nano Letters*, 2008, **8**, 2458–2462,[139] Copyright 2008 American Chemical Society. (c) Reproduced from Lee *et al.*, Elastic and frictional properties of graphene, *Physica Status Solidi: B*, 2009, **246**, 2562–2567,[140] John Wiley and Sons, © WILEY-VCH Verlag GmbH & Co. KGaA, Weinheim.

an enclosed cavity. Subsequently, the cavity with the film is transferred into a special atmosphere (N_2, inert gas, or compressed air) in order to achieve a pressure difference between the inside and outside of the cavity, whereby deformation of the film occurs. According to the relation between the pressure difference and the displacement of the film center, the elastic modulus can be determined. In 2008, Bunch *et al.*[139] determined the elastic constant and weight of a single layer of graphene by this method, and the Young modulus was calculated to be 1 TPa. Recently, the nanoindentation method with the aid of AFM has become more and more popular. First, micron-sized circular holes are covered with a graphene film, followed by the load of the AFM tip on the center of the graphene film to measure the force-displacement behavior of the film. The elastic modulus can be eventually determined from the non-linear stress–strain curve. This method was firstly studied by Lee *et al.*[27] to measure the elastic properties and intrinsic strength of monolayer graphene. High second- and third-elastic constants were recorded to be 340 and 690 N m^{-1}, respectively. The breaking strength was *ca.* 42 N m^{-1}, which is much stronger than that of steel of the same thickness. The Young modulus was determined to be 1 TPa, making graphene one of the strongest materials ever. Lee's further research[140] proved that the elastic modulus of single, double, and triple layers of graphene are all consistent within the range of allowable error.

1.4 Challenges for the Development of Chemically Derived Graphene

1.4.1 Technical Challenges

As discussed in Section 1.2, numerous methods have been developed to synthesize CDG in laboratories and industry. Comprehensive reviews on the preparation of CDG at laboratory and industrial scale are available in the literature.[51,141,142] Liquid phase exfoliation and chemical oxidation–exfoliation–reduction of graphite are the two most important methods used for the large scale production of CDG. Although around a few tens of start-up companies have pursued the production of CDG on a ton scale, the technology is still in its early stages and challenges are still faced by CDG manufacturers. A huge number of strong oxidants and reductants are needed for the chemical oxidation and reduction of graphite, such as H_2SO_4, $KMnO_4$, hydrazine, or $NaBH_4$. These chemical reagents impose serious pollution issues and cannot be recycled with the existing technology, which also increases the financial burden of CDG producers. In addition, incomplete reduction leads to five or seven membered rings and other structural defects, which cannot be removed completely even after high-temperature annealing. The presence of interrupted sp^2-hybridized C–C bonds results in poor-quality CDG materials. Liquid phase exfoliation affords CDG with better quality; however, the CDG usually presents thick graphene layers and suffer from solvent or surfactant contamination. On top of the already-mentioned drawbacks, product inconsistency (in terms of the chemical and physical properties of CDG)

from batch to batch remains a major problem in both methods. Therefore, the development of processes to produce high-quality CDG with facile, cost-efficient, and environmental-friendly methodologies remains a challenge for researchers. One direction is to identify suitable ways to weaken and overcome the van der Waals forces so as to achieve the exfoliation of graphene layers with minimum effort. The use of non-toxic chemical reagents with a highly integrated and efficient production line is also important.

1.4.2 Economic Challenges

The cost-to-performance ratio is a critical factor that determines a product's commercial value. Products with low cost-to-performance ratios are likely to attract the market's attention and thus lead to potential success. In view of the special features and many potential applications of CDG, the manufacturing of CDG differs from that of other products. 'Application-oriented' production should be adopted instead of the mass production of a single product at once. This is analogous to the case of certain semiconductor manufacturers, where a few ten or hundred types of products can be produced with a few production lines, and the production volume of each product depends on the customer and market demand. In addition to the cost of the methods for the production of CDG mentioned in the previous paragraph, the ability to handle and produce a range of CDG products for different applications with the existing production capability will also positively contribute to the competitive and fast changing market demand. Efficient communication with customers and an appropriate marketing plan is important. On top of that, the gradual improvement of the entire industrial chain is highly desired. The storage and transportation of the raw material and products are two areas to be considered. The storage and transportation of CDG in its wet or dry form has to be considered, together with its subsequent usage and applications. For example, storage of CDG suspensions at low concentrations usually requires a large space. The extra volume and weight from the solvent greatly increases the cost of storage and transportation. As for CDG in the form of powder, aggregation is believed to be the biggest challenge. In addition, fine powders present serious health and safety concerns. Thus, CDG manufacturers have to adopt different storage and transportation methods to meet the specific requirements of customers in order to improve their profits.

In the past five years, the number of graphene-related patent has quickly risen. Up to April 2015, the number of global graphene patents amounted to 13 923. However, the patents are mainly focused on low-value products. Patents dealing with semiconductor devices, touchscreens, sensors, bio-pharmaceuticals, and other high-value fields are relatively scarce. Most research work relevant to these fields is still in the laboratory stage. The gap between the industry demand and laboratory research seriously hinders the progress of the graphene industry, which, in turn, lessens the enthusiasm of graphene investigation, forming a vicious cycle. In view of the above, more attention and funds should be allocated to research driving for high-value products and cost-efficient and sustainable production.

Presently, upstream enterprises make a living by selling low-quality natural graphite at the price of a few hundred dollars per ton, while the price of high-quality graphene composites is more than 10 000 dollars per ton. Due to the limitations of the current graphene preparation methods, the performance of the products is not stable and the price is relatively high. Thus, most downstream enterprises are at the stage of wait and see, leading to a 'communication breakdown' between upstream and downstream enterprises. This impacts negatively the graphene industry chain. In addition, standards with respect to the product specification and quality classification in the graphene industry have not yet been established. Meanwhile, the majority of the graphene R&D work is still research institution- and university-based, who rely on state funding since enterprises lack the necessary money. This makes market demand-driven and applied research less attractive, since high-impact journal papers mainly focus on cutting-edge research with potential applications only many years later. Most enterprises are still unable to find a stable business model and profit model, and this is the biggest challenge all graphene manufacturers are currently facing.

1.4.3 Environmental and Safety Challenges

The biggest environmental problem that the graphene industry faces is the chemical reagents used in the fabrication of CDG. The treatment of these chemical reagents at the laboratory scale does not seem to be a big problem. Therefore, little attention has been paid to the subsequent waste treatment at the laboratory scale and thus, little concerns are imposed when researchers develop 'new' methods in their labs. This is another indication of the lack of a 'bridge' between lab research and industry application.

Apart from the chemical reagents used during production, the potential risks of CDG materials on the human body are also a huge challenge for the promotion of the graphene industry. For an emerging industry, any potential or uncertain health risk may greatly hider its development because of the increasing health and safety awareness. Although material safety data sheets (MSDS) for CDG and relevant products can be found on some manufacturer's websites, there are no specific health and safety regulations related to CDG. There is also no clear and strong scientific evidence to determine the potential safety effects of CDG and its composite materials and to eliminate public worries concerning graphene. Fortunately, certain existing regulations can serve as guidance and reference, such as the REACH Regulation, which has been set up for the estimation and supervision of nanomaterial safety issues. The U.S. Department of Health and Human Services has been conducting a project on 'The Impact of Graphene-based Nanomaterials on Public Health' since 2014. This project addresses the ways to assess the potential health impacts of the use of carbon nanomaterials by using well-defined and validated methods for the detection and measurement of graphene in blood and other body fluids to determine where particles are deposited and how they are cleared from the body. It also explores the effects of graphene on the

immune system markers and the nervous system. Besides in-depth understanding of toxicological mechanisms, appropriate risk management methods should be established as soon as possible. The highest concentration of graphene powder in the workspace and the longest time of exposure should be standardized to minimize the effect on workers. At last, an optimized production flow can help reduce the risks of graphene-related materials, such as the storage and transportation of graphene in the form of intermediate products. Of course, the relationship between safety issues and the customer's demands needs to be carefully balanced.

References

1. W. S. Hummers and R. E. Offeman, *J. Am. Chem. Soc.*, 1958, **80**, 1339.
2. L. Staudenmaier, *Eur. J. Inorg. Chem.*, 1898, **31**, 1481–1487.
3. B. C. Brodie, *Ann. Chim. Phys.*, 1860, **59**, 466–472.
4. S. Stankovich, D. A. Dikin, R. D. Piner, K. A. Kohlhaas, A. Kleinhammes, Y. Y. Jia, Y. Wu, S. T. Nguyen and R. S. Ruoff, *Carbon*, 2007, **45**, 1558–1565.
5. X. Huang, X. Y. Qi, F. Boey and H. Zhang, *Chem. Soc. Rev.*, 2012, **41**, 666–686.
6. J.-M. Yun, J.-S. Yeo, J. Kim, H.-G. Jeong, D.-Y. Kim, Y.-J. Noh, S.-S. Kim, B.-C. Ku and S.-I. Na, *Adv. Mater.*, 2011, **23**, 4923–4928.
7. S. Park, J. An, J. R. Potts, A. Velamakanni, S. Murali and R. S. Ruoff, *Carbon*, 2011, **49**, 3019–3023.
8. V. H. Pham, T. V. Cuong, T.-D. Nguyen-Phan, H. D. Pham, E. J. Kim, S. H. Hur, E. W. Shin, S. Kim and J. S. Chung, *Chem. Commun.*, 2010, **46**, 4375–4377.
9. H.-J. Shin, K. K. Kim, A. Benayad, S.-M. Yoon, H. K. Park, I.-S. Jung, M. H. Jin, H.-K. Jeong, J. M. Kim, J.-Y. Choi and Y. H. Lee, *Adv. Funct. Mater.*, 2009, **19**, 1987–1992.
10. C. K. Chua and M. Pumera, *J. Mater. Chem. A*, 2013, **1**, 1892–1898.
11. F. Z. Jun, W. Kai, Y. Jun, W. Tong, Z. L. Jie, F. Jing, R. Y. Ming, S. L. Ping and W. Fei, *ACS Nano*, 2011, **5**, 191–198.
12. F. Z. Jun, W. Kai, W. Tong, Y. Jun, S. L. Ping and S. Bo, *Carbon*, 2010, **48**, 1670–1692.
13. P. B. Liu, Y. Huang and L. Wang, *Mater. Lett.*, 2013, **91**, 125–128.
14. G. X. Wang, J. Yang, J. Park, X. L. Gou, B. Wang, H. Liu and J. Yao, *J. Phys. Chem. C*, 2008, **112**, 8192–8195.
15. J. L. Zhang, H. J. Yang, G. X. Shen, P. Cheng, J. Y. Zhang and S. W. Guo, *Chem. Commun.*, 2010, **46**, 1112–1114.
16. P. Solís-Fernández, R. Rozada, J. I. Paredes, S. Villar-Rodil, M. J. Fernández-Merino, L. Guardia, A. Martínez-Alonso and J. M. D. Tascón, *J. Alloys Compd.*, 2012, **536**, S532–S537.
17. M. J. Fernández-Merino, L. Guardia, J. I. Paredes, S. Villar-Rodil, P. Solís-Fernández, A. Martínez-Alonso and J. M. D. Tascón, *J. Phys. Chem. C*, 2010, **114**, 6426–6432.

18. O. Akhavan, M. Kalaee, Z. S. Alavi, S. M. A. Ghiasi and A. Esfandiar, *Carbon*, 2012, **50**, 3015–3025.
19. X. B. Fan, W. C. Peng, Y. Li, X. Y. Li, S. L. Wang, G. L. Zhang and F. B. Zhang, *Adv. Mater.*, 2008, **20**, 4490–4493.
20. C. Z. Zhu, S. J. Guo, Y. X. Fang and S. J. Dong, *ACS Nano*, 2010, **4**, 2429–2437.
21. S. F. Pei, J. P. Zhao, J. H. Du, W. C. Ren and H.-M. Cheng, *Carbon*, 2010, **48**, 4466–4474.
22. J. P. Zhao, S. F. Pei, W. C. Ren, L. B. Gao and H. M. Cheng, *ACS Nano*, 2010, **4**, 5245–5252.
23. X. L. Fu, T. T. Lou, Z. P. Chen, M. Lin, W. W. Feng and L. X. Chen, *ACS Appl. Mater. Interfaces*, 2012, **4**, 1080–1086.
24. H. K. Chae, D. Y. Siberio-Pérez, J. Kim, Y. Go, M. Eddaoudi, A. J. Matzger, M. O'Keeffe and O. M. Yaghi, *Nature*, 2004, **427**, 523–527.
25. A. K. Geim, *Science*, 2009, **324**, 1530–1534.
26. R. R. Nair, P. Blake, A. N. Grigorenko, K. S. Novoselov, T. J. Booth, T. Stauber, N. M. R. Peres and A. K. Geim, *Science*, 2008, **320**, 1308.
27. C. Lee, X. D. Wei, J. W. Kysar and J. Hone, *Science*, 2008, **321**, 385–388.
28. A. A. Balandin, S. Ghosh, W. Z. Bao, I. Calizo, D. Teweldebrhan, F. Miao and C. N. Lau, *Nano Lett.*, 2008, **8**, 902–907.
29. W. C. Ren and H. M. Cheng, *Nat. Nanotechnol.*, 2014, **9**, 726–730.
30. S. Stankovich, R. D. Piner, X. Chen, N. Wu, S. T. Nguyen and R. S. Ruoff, *J. Mater. Chem.*, 2006, **16**, 155–158.
31. D. Li, M. B. Muller, S. Gilje, R. B. Kaner and G. G. Wallace, *Nat. Nanotechnol.*, 2008, **3**, 101–105.
32. X. Zhou, J. Zhang, H. Wu, H. Yang, J. Zhang and S. Guo, *J. Phys. Chem. C*, 2011, **115**, 11957–11961.
33. M. Zhou, Y. Wang, Y. Zhai, J. Zhai, W. Ren, F. Wang and S. Dong, *Chemistry*, 2009, **15**, 6116–6120.
34. Y. Zhou, Q. Bao, L. A. L. Tang, Y. Zhong and K. P. Loh, *Chem. Mater.*, 2009, **21**, 2950–2956.
35. H. L. Wang, J. T. Robinson, X. L. Li and H. J. Dai, *J. Am. Chem. Soc.*, 2009, **131**, 9910–9911.
36. X. Wang, P. F. Fulvio, G. A. Baker, G. M. Veith, R. R. Unocic, S. M. Mahurin, M. Chi and S. Dai, *Chem. Commun.*, 2010, **46**, 4487–4489.
37. D. Nuvoli, L. Valentini, V. Alzari, S. Scognamillo, S. B. Bon, M. Piccinini, J. Illescas and A. Mariani, *J. Mater. Chem.*, 2011, **21**, 3428–3431.
38. Y. Hernandez, V. Nicolosi, M. Lotya, F. M. Blighe, Z. Sun, S. De, I. T. McGovern, B. Holland, M. Byrne, Y. K. Gun'Ko, J. J. Boland, P. Niraj, G. Duesberg, S. Krishnamurthy, R. Goodhue, J. Hutchison, V. Scardaci, A. C. Ferrari and J. N. Coleman, *Nat. Nanotechnol.*, 2008, **3**, 563–568.
39. A. O'Neill, U. Khan, P. N. Nirmalraj, J. Boland and J. N. Coleman, *J. Phys. Chem. C*, 2011, **115**, 5422–5428.
40. W. W. Liu and J. N. Wang, *Chem. Commun.*, 2011, **47**, 6888–6890.
41. W. Du, J. Lu, P. Sun, Y. Zhu and X. Jiang, *Chem. Phys. Lett.*, 2013, **568–569**, 198–201.

42. C. Knieke, A. Berger, M. Voigt, R. N. K. Taylor, J. Röhrl and W. Peukert, *Carbon*, 2010, **48**, 3196–3204.
43. W. F. Zhao, F. Ming, F. R. Wu, H. Wu, L. W. Wang and G. H. Chen, *J. Mater. Chem.*, 2010, **20**, 5817–5819.
44. V. León, A. M. Rodriguez, P. Prieto, M. Prato and E. Vázquez, *ACS Nano*, 2014, **8**, 563–571.
45. I.-Y. Jeon, H.-J. Choi, S.-M. Jung, J.-M. Seo, M.-J. Kim, L. M. Dai and J.-B. Baek, *J. Am. Chem. Soc.*, 2013, **135**, 1386–1393.
46. I.-Y. Jeon, Y.-R. Shin, G.-J. Sohn, H.-J. Choi, S.-Y. Bae, J. Mahmood, S.-M. Jung, J.-M. Seo, M.-J. Kim, D. W. Chang, L. M. Dai and J.-B. Baek, *Proc. Natl. Acad. Sci.*, 2012, **109**, 5588–5593.
47. N. I. Kovtyukhova, Y. Wang, A. Berkdemir, R. Cruz-Silva, M. Terrones, V. H. Crespi and T. E. Mallouk, *Nat. Chem.*, 2014, **6**, 957–963.
48. W. J. Fu, J. Kiggans, S. H. Overbury, V. Schwartz and C. D. Liang, *Chem. Commun.*, 2011, **47**, 5265–5267.
49. A. V. Okotrub, E. O. Fedorovskaya, B. V. Senkovskiy and L. G. Bulusheva, *Phys. Status Solidi B*, 2015, **252**, 2444–2450.
50. H. Huang, Y. Xia, X. Y. Tao, J. Du, J. W. Fang, Y. P. Gan and W. K. Zhang, *J. Mater. Chem.*, 2012, **22**, 10452–10456.
51. Y. Zhu, H. Ji, H.-M. Cheng and R. S. Ruoff, *Natl. Sci. Rev.*, 2018, DOI: 10.1093/nsr/nwx055.
52. L. Jiang and Z. Fan, *Nanoscale*, 2014, **6**, 1922–1945.
53. L. L. Zhang, X. Zhao, M. D. Stoller, Y. Zhu, H. Ji, S. Murali, Y. Wu, S. Perales, B. Clevenger and R. S. Ruoff, *Nano Lett.*, 2012, **12**, 1806–1812.
54. Y. W. Zhu, S. Murali, M. D. Stoller, K. J. Ganesh, W. W. Cai, P. J. Ferreira, A. Pirkle, R. M. Wallace, K. A. Cychosz, M. Thommes, D. Su, E. A. Stach and R. S. Ruoff, *Science*, 2011, **332**, 1537–1541.
55. Z.-S. Wu, W. Ren, L. Xu, F. Li and H.-M. Cheng, *ACS Nano*, 2011, **5**, 5463–5471.
56. S. Wu and Y. Zhu, *Sci. China Mater.*, 2017, **60**, 25–38.
57. X. Yang, C. Cheng, Y. Wang, L. Qiu and D. Li, *Science*, 2013, **341**, 534–537.
58. K. Zhang, L. L. Zhang, X. Zhao and J. Wu, *Chem. Mater.*, 2010, **22**, 1392–1401.
59. C. Toro and J. M. Buriak, *Chem. Mater.*, 2017, **29**, 4607–4608.
60. R. Verdejo, M. M. Bernal, L. J. Romasanta and M. A. Lopez-Manchado, *J. Mater. Chem.*, 2011, **21**, 3301–3310.
61. Y. Fan, L. Wang, J. Li, J. Li, S. Sun, F. Chen, L. Chen and W. Jiang, *Carbon*, 2010, **48**, 1743–1749.
62. O. Tapasztó, L. Tapasztó, M. Markó, F. Kern, R. Gadow and C. Balázsi, *Chem. Phys. Lett.*, 2011, **511**, 340–343.
63. K. Wang, Y. Wang, Z. Fan, J. Yan and T. Wei, *Mater. Res. Bull.*, 2011, **46**, 315–318.
64. C. Ramírez, S. M. Vega-Diaz, A. Morelos-Gómez, F. M. Figueiredo, M. Terrones, M. I. Osendi, M. Belmonte and P. Miranzo, *Carbon*, 2013, **57**, 425–432.
65. C. Ramirez, F. M. Figueiredo, P. Miranzo, P. Poza and M. I. Osendi, *Carbon*, 2012, **50**, 3607–3615.

66. G. M. Scheuermann, L. Rumi, P. Steurer, W. Bannwarth and R. Mülhaupt, *J. Am. Chem. Soc.*, 2009, **131**, 8262–8270.
67. H. M. A. Hassan, V. Abdelsayed, A. E. R. S. Khder, K. M. AbouZeid, J. Terner, M. S. El-Shall, S. I. Al-Resayes and A. A. El-Azhary, *J. Mater. Chem.*, 2009, **19**, 3832–3837.
68. S. J. Guo, S. J. Dong and E. Wang, *ACS Nano*, 2010, **4**, 547–555.
69. S. Zhang, Y. Shao, H.-g. Liao, J. Liu, I. A. Aksay, G. Yin and Y. Lin, *Chem. Mater.*, 2011, **23**, 1079–1081.
70. Y. Hu, H. Zhang, P. Wu, H. Zhang, B. Zhou and C. Cai, *PCCP Phys. Chem. Chem. Phys.*, 2011, **13**, 4083–4094.
71. F. Ren, H. Wang, C. Zhai, M. Zhu, R. Yue, Y. Du, P. Yang, J. Xu and W. Lu, *ACS Appl. Mater. Interfaces*, 2014, **6**, 3607–3614.
72. Z.-x. Cai, C.-c. Liu, G.-h. Wu, X.-m. Chen and X. Chen, *Electrochim. Acta*, 2014, **127**, 377–383.
73. R. Wang, Z. Wu, C. Chen, Z. Qin, H. Zhu, G. Wang, H. Wang, C. Wu, W. Dong, W. Fan and J. Wang, *Chem. Commun.*, 2013, **49**, 8250–8252.
74. W. J. Hong, H. Bai, Y. X. Xu, Z. Y. Yao, Z. Z. Gu and G. Q. Shi, *J. Phys. Chem. C*, 2010, **114**, 1822–1826.
75. J. Luo, S. Jiang, H. Zhang, J. Jiang and X. Liu, *Anal. Chim. Acta*, 2012, **709**, 47–53.
76. W. Yuan, Y. Gu and L. Li, *Appl. Surf. Sci.*, 2012, **261**, 753–758.
77. X. Liu, X. W. Zhang, J. H. Meng, H. L. Wang, Z. G. Yin, J. L. Wu and H. L. Gao, *Nanotechnology*, 2014, **25**, 365602.
78. M. Bastwros, G.-Y. Kim, C. Zhu, K. Zhang, S. R. Wang, X. D. Tang and X. W. Wang, *Composites, Part B*, 2014, **60**, 111–118.
79. C.-H. Jeon, Y.-H. Jeong, J.-J. Seo, H. N. Tien, S.-T. Hong, Y.-J. Yum, S.-H. Hur and K.-J. Lee, *Int. J. Precis. Eng. Manuf.*, 2014, **15**, 1235–1239.
80. S. J. Yan, S. L. Dai, X. Y. Zhang, C. Yang, Q. H. Hong, J. Z. Chen and Z. M. Lin, *Mater. Sci. Eng. A*, 2014, **612**, 440–444.
81. X. Huang, X. Zhou, S. Wu, Y. Wei, X. Qi, J. Zhang, F. Boey and H. Zhang, *Small*, 2010, **6**, 513–516.
82. R. Awasthi and R. N. Singh, *Carbon*, 2013, **51**, 282–289.
83. R. Muszynski, B. Seger and P. V. Kamat, *J. Phys. Chem. C*, 2008, **112**, 5263–5266.
84. H. M. Liu and W. S. Yang, *Energy Environ. Sci.*, 2011, **4**, 4000–4008.
85. J. S. Bonso, A. Rahy, S. D. Perera, N. Nour, O. Seitz, Y. J. Chabal, K. J. Balkus, J. P. Ferraris and D. J. Yang, *J. Power Sources*, 2012, **203**, 227–232.
86. X. Shen, J. Wu, S. Bai and H. Zhou, *J. Alloys Compd.*, 2010, **506**, 136–140.
87. S. K. Behera, *Chem. Commun.*, 2011, **47**, 10371–10373.
88. Y. Ye, T. Kong, X. Yu, Y. Wu, K. Zhang and X. Wang, *Talanta*, 2012, **89**, 417–421.
89. C. Chen, W. Fu and C. Yu, *Mater. Lett.*, 2012, **82**, 133–136.
90. Y. M. He, W. J. Chen, X. D. Li, Z. X. Zhang, J. C. Fu, C. H. Zhao and E. Q. Xie, *ACS Nano*, 2013, **7**, 174–182.
91. J. Yan, Z. Fan, T. Wei, W. Qian, M. Zhang and F. Wei, *Carbon*, 2010, **48**, 3825–3833.

92. B. Wang, Y. Wang, J. Park, H. Ahn and G. Wang, *J. Alloys Compd.*, 2011, **509**, 7778–7783.
93. C. W. Sun, F. Li, C. Ma, Y. Wang, Y. L. Ren, W. Yang, Z. H. Ma, J. Q. Li, Y. J. Chen, Y. Kim and L. Q. Chen, *J. Mater. Chem. A*, 2014, **2**, 7188–7196.
94. Q. Y. Liao, N. Li, S. X. Jin, G. W. Yang and C. X. Wang, *ACS Nano*, 2015, **9**, 5310–5317.
95. Y.-X. Wang, Y.-G. Lim, M.-S. Park, S.-L. Chou, J. H. Kim, H.-K. Liu, S.-X. Dou and Y.-J. Kim, *J. Mater. Chem. A*, 2014, **2**, 529–534.
96. H. Zhang, J. C. Feng, T. Fei, S. Liu and T. Zhang, *Sens. Actuators, B*, 2014, **190**, 472–478.
97. X. Yang, M. S. Xu, W. M. Qiu, X. Q. Chen, M. Deng, J. L. Zhang, H. Iwai, E. Watanabe and H. Z. Chen, *J. Mater. Chem.*, 2011, **21**, 8096–8103.
98. F.-A. He, J.-T. Fan, F. Song, L.-M. Zhang and H. Lai-Wa Chan, *Nanoscale*, 2011, **3**, 1182–1188.
99. G. X. Zhu, Y. J. Liu, Z. Xu, T. Jiang, C. Zhang, X. Li and G. Qi, *ChemPhysChem*, 2010, **11**, 2432–2437.
100. D. Y. Zhai, B. H. Li, H. D. Du, G. Y. Gao, L. Gan, Y. B. He, Q. H. Yang and F. Y. Kang, *Carbon*, 2012, **50**, 5034–5043.
101. J. Huang, L. M. Zhang, B. Chen, N. Ji, F. H. Chen, Y. Zhang and Z. J. Zhang, *Nanoscale*, 2010, **2**, 2733–2738.
102. H. L. Wang, H. S. Casalongue, Y. Y. Liang and H. J. Dai, *J. Am. Chem. Soc.*, 2010, **132**, 7472–7477.
103. S. Hassan, M. Suzuki and A. A. E. El-Moneim, *Int. J. Electrochem. Sci.*, 2014, **9**, 8340–8354.
104. Y. Yang, J. Q. Li, D. Q. Chen and J. B. Zhao, *ACS Appl. Mater. Interfaces*, 2016, **8**, 26730–26739.
105. T. Hu, G. Q. Xin, H. T. Sun, X. Sun, M. P. Yu, C. S. Liu and J. Lian, *RSC Adv.*, 2014, **4**, 1521–1525.
106. C. L. Fu, T. Q. Chen, W. Qin, T. Lu, Z. Sun, X. H. Xie and L. K. Pan, *Ionics*, 2015, **22**, 555–562.
107. C. Y. Ho, R. W. Powell and P. E. Liley, *Thermal Conductivity of the Elements: A Comprehensive Review*, National Standard Reference Data System, 1974.
108. P. G. Klemens and D. F. Pedraza, *Carbon*, 1994, **32**, 735–741.
109. S. Berber, Y.-K. Kwon and D. Tománek, *Phys. Rev. Lett.*, 2000, **84**, 4613–4616.
110. D. L. Nika, E. P. Pokatilov, A. S. Askerov and A. A. Balandin, *Phys. Rev. B*, 2009, **79**, 155413.
111. F. Hao, D. N. Fang and Z. P. Xu, *Appl. Phys. Lett.*, 2011, **99**, 041901.
112. J. H. Seol, I. Jo, A. L. Moore, L. Lindsay, Z. H. Aitken, M. T. Pettes, X. Li, Z. Yao, R. Huang and D. Broido, *Science*, 2010, **328**, 213–216.
113. H. Malekpour, K.-H. Chang, J.-C. Chen, C.-Y. Lu, D. Nika, K. Novoselov and A. Balandin, *Nano Lett.*, 2014, **14**, 5155–5161.
114. J. D. Renteria, S. Ramirez, H. Malekpour, B. Alonso, A. Centeno, A. Zurutuza, A. I. Cocemasov, D. L. Nika and A. A. Balandin, *Adv. Funct. Mater.*, 2015, **25**, 4664–4672.

115. C. Punckt, F. Muckel, S. Wolff, I. A. Aksay, C. A. Chavarin, G. Bacher and W. Mertin, *Appl. Phys. Lett.*, 2013, **102**, 023114.
116. J.-A. Yan and M. Y. Chou, *Phys. Rev. B*, 2010, **82**, 125403.
117. M. D. Stoller, S. Park, Y. W. Zhu, J. An and R. S. Ruoff, *Nano Lett.*, 2008, **8**, 3498–3502.
118. L. L. Zhang, X. Zhao, H. X. Ji, M. D. Stoller, L. F. Lai, S. Murali, S. McDonnell, B. Cleveger, R. M. Wallace and R. S. Ruoff, *Energy Environ. Sci.*, 2012, **5**, 9618–9625.
119. L. L. Zhang, X. Zhao, H. Ji, M. D. Stoller, L. Lai, S. Murali, S. Mcdonnell, B. Cleveger, R. M. Wallace and R. S. Ruoff, *Energy Environ. Sci.*, 2012, **5**, 9618–9625.
120. E. Pollak, B. Geng, K.-J. Jeon, I. T. Lucas, T. J. Richardson, F. Wang and R. Kostecki, *Nano Lett.*, 2010, **10**, 3386–3388.
121. E. Yoo, J. Kim, E. Hosono, H.-s. Zhou, T. Kudo and I. Honma, *Nano Lett.*, 2008, **8**, 2277–2282.
122. D. Pan, S. Wang, B. Zhao, M. Wu, H. Zhang, Y. Wang and Z. Jiao, *Chem. Mater.*, 2009, **21**, 3136–3142.
123. D. Geng, Y. Chen, Y. Chen, Y. Li, R. Li, X. Sun, S. Ye and S. Knights, *Energy Environ. Sci.*, 2011, **4**, 760–764.
124. L. Zhang and Z. Xia, *J. Phys. Chem. C*, 2011, **115**, 11170–11176.
125. L. Yang, S. Jiang, Y. Zhao, L. Zhu, S. Chen, X. Wang, Q. Wu, J. Ma, Y. Ma and Z. Hu, *Angew. Chem.*, 2011, **50**, 7132–7135.
126. M. D. Esrafili, R. Mohammad-Valipour, S. M. Mousavi-Khoshdel and P. Nematollahi, *ChemPhysChem*, 2015, **16**, 3719–3727.
127. G. Kalita, K. Wakita, M. Takahashi and M. Umeno, *J. Mater. Chem.*, 2011, **21**, 15209–15213.
128. Z. H. Sheng, L. Shao, J.-J. Chen, W. J. Bao, F.-B. Wang and X. H. Xia, *ACS Nano*, 2011, **5**, 4350–4358.
129. L. S. Chen, X. Z. Cui, Y. X. Wang, M. Wang, R. H. Qiu, Z. Shu, L. X. Zhang, Z. L. Hua, F. M. Cui, C. Y. Wei and J. L. Shi, *Dalton Trans.*, 2014, **43**, 3420–3423.
130. J. Liang, Y. Jiao, M. Jaroniec and S. Z. Qiao, *Angew. Chem.*, 2012, **51**, 11496–11500.
131. J. Han, J. Y. Cheon, S. H. Joo and S. Park, *Solid State Sci.*, 2014, **33**, 1–5.
132. Y. R. Sun, C. Y. Du, G. K. Han, Y. T. Qu, L. Du, Y. J. Wang, G. Y. Chen, Y. Z. Gao and G. P. Yin, *Electrochim. Acta*, 2016, **212**, 313–321.
133. E. Konstantinova, S. O. Dantas and P. M. V. B. Barone, *Phys. Rev. B*, 2006, **74**, 035417.
134. G. V. Lier, C. V. Alsenoy, V. V. Doren and P. Geerlings, *Chem. Phys. Lett.*, 2000, **326**, 181–185.
135. Y. Huang, J. Wu and K. C. Hwang, *Phys. Rev. B*, 2006, **74**, 245413.
136. C. Gómez-Navarro, M. Burghard and K. Kern, *Nano Lett.*, 2008, **8**, 2045–2049.
137. I. W. Frank, D. M. Tanenbaum, A. M. v. d. Zande and P. L. McEuen, *J. Vac. Sci. Technol., B: Microelectron. Nanometer Struct.*, 2007, **25**, 2558–2561.

138. J. J. Vlassak and W. D. Nix, *J. Mater. Res.*, 1992, **7**, 3242–3249.
139. J. S. Bunch, S. S. Verbridge, J. S. Alden, A. M. v. d. Zande, J. M. Parpia, H. G. Craighead and P. L. McEuen, *Nano Lett.*, 2008, **8**, 2458–2462.
140. C. Lee, X. Wei, Q. Li, R. Carpick, J. W. Kysar and J. Hone, *Phys. Status Solidi B*, 2009, **246**, 2562–2567.
141. M. J. Allen, V. C. Tung and R. B. Kaner, *Chem. Rev.*, 2009, **110**, 132–145.
142. Y. W. Zhu, S. Murali, W. W. Cai, X. S. Li, J. W. Suk, J. R. Potts and R. S. Ruoff, *Adv. Mater.*, 2010, **22**, 3906–3924.